UNIVERSIDADE DE SÃO PAULO

INSTITUTO DE FÍSICA
CAIXA POSTAL 20516
01498 - SÃO PAULO - SP
BRASIL

PUBLICAÇÕES

IFUSP/P-520

OPTICAL ABSORPTION SPECTROSCOPY OF NATURAL AND IRRADIATED PINK TOURMALINE

by

Marly Bueno de Camargo and Sadao Isotani
Instituto de Física, Universidade de São Paulo

Março/1985

OPTICAL ABSORPTION SPECTROSCOPY OF NATURAL AND IRRADIATED PINK TOURMALINE

Marly Bueno de Camargo and Sadao Isotani

Instituto de Física, Universidade de São Paulo
C.P. 20.516, São Paulo, SP, Brazil

ABSTRACT

We have studied the Brazilian natural pink tourmaline through the polarized optical absorption measurements. The effect of increasing doses of γ-rays from ^{60}Co in the spectra were determined (maximum of 20 MGy). The following optical absorption bands were observed: 8,500 and 14,800 cm^{-1} assigned to d-d transitions of Fe^{2+} in b- and c-sites, respectively; 19,500 and 25,500 cm^{-1} assigned to $^5E \rightarrow {}^5A_1$ and $^5B_2 \rightarrow {}^5A_1$ d-d transitions of Mn^{3+}, respectively.

Key Words: Tourmaline, Optical Absorption, Radiation Effects.

I. INTRODUCTION

Tourmaline is a mineral belonging to the silicate class, whose chemical composition $NaX_3Al_6B_3Si_6O_{27}(OH,F)_4$, is extremely complex. The X-sites can be occupied by several ions which explains the great number of varieties in the kinds of tourmaline found in nature. They can be grouped in series among the species: (a) dravite, where X = Mg; (b) schorl, where X = = Fe,Mn; (c) elbaite, where X = Li, Al. There is a continuous series between schorl and elbaite and another one between dravite and schorl. There is a gap between dravite and elbaite which can be observed in the comparison between the lattice parameters a and c obtained by Barton[1]. Tourmaline has a hardness 7 on the Mohs scale. Its space group[2-4] is R_{3m}. In general the crystals are prismatic with a trigonal prism and another hexagonal prism of second order subordinated to it. Its density ranges from 3.02 to 3.26 g/cm^3 and the refractive indexes are ranging between 1.62 - 1.64. The unit cell dimensions vary: a from 15.84 to 16.03 Å and c from 7.10 to 7.25 Å. There is a lot of studies on the structure of tourmaline through the X-ray diffraction[5-10].

Pink tourmaline is an elbaite. One can see its central segment including the brucite structure in Figure 1.

Insert Figure 1

The b-site contains the X atom of the $XO_4(OH,F)_2$-structure which is slightly distorted and the c-site contains the Al atom of $AlO_5(OH,F)$-structure, highly distorted[6].

The color of pink tourmaline[11] is due to the absorption of light in the green-yellow and blue-violet areas of the spectrum

so that the emergent light from the crystal is enriched on the red and green-blue, resulting in a purple pink tonality. This color is strongly pleochromatic, intensified in the direction of c-axis of the crystal. The color also changes in intensity and tonality from sample to sample. The origin of the color of pink tourmalines has been for a long time the subject of discussion among mineralogists[12].

In the pink tourmaline both manganese and iron are present. However, the iron concentration is generally low[11,13]. The color is probably due to the absorption of light by the manganese cations.

The pink tourmaline presents several absorption bands between 5,000 and 30,000 cm^{-1}, which have been extensively studied[4,12,14-18]. In the Table 1 we present the bands observed and their respective assignments. We can notice that there are bands whose assignments are still indefinite, mainly refering to the 19,000 cm^{-1} band, which together with the UV band edge is responsible for the color.

Insert Table 1

There are lots of pink tourmaline species, each one reacting differently to the irradiation and annealing process[19]. Studies about the effects of irradiation and heating on the tourmalines were performed qualitatively only for the 19,500 cm^{-1} band. It was observed that the color of the pink tourmaline can be emphasized and sometimes a yellow color mixed to the pre-existent pink one appeared, after the irradiation process. The heating at 500°C eliminates the pink color, but the yellow color is not affected.

Our main objective is to present a comparative study by optical absorption of three kinds of pink tourmaline from Minas Gerais, Brasil and one green sample from Goiás, Brasil. We used initially natural gemstones, and which were later on irradiated with γ-rays from a ^{60}Co source.

II. EXPERIMENTAL

The crystals presented elongated prismatic shape and with the external surface grooved along the crystallographic axis c. Their cross section is rounded triangle.

The impurity concentrations of manganese and iron are indicated in Table 2.

Insert Table 2

The data show that in the pink tourmalines the manganese concentration is higher than the iron's while in the green tourmalines both manganese and iron are found in the same high proportion.

The samples were cut by a 0.012" thick diamond edged saw isomet from Buehler Co. The polishing was first carried out with sandpaper of decreasing granulation 180, 320, 400 and 600, and afterwards with Alumina in a politrix Minimet Buehler Co.

The slices used in the experiments had a thickness ranging from 0.65 - 1.65 mm. They were cut either parallel or perpendicular to the c-axis.

A Carl-Zeiss DMR 21 spectrophotometer was used for the optical absorption measurements. Polarized light measurements

were done with Type II polaroid.

The measurements were done using the samples cut in the same way as in Figure 2.

Insert Figure 2

The samples were γ-irradiated using a ^{60}Co-source from EMBRARAD*. The dose was controlled by means of three processes: Ceric-Cerous dosimetric system, AECL Red Acrylic dosimetric system and UKAEA Red Perspex dosimeter.

III. RESULTS OF THE OPTICAL ABSORPTION MEASUREMENTS

The non-polarized absorption spectra of the tourmalines A_1, A_2 and A_3 are shown in Figure 3. For those measurements we used slices of pink tourmaline cut parallel to the (001) plane, so that $\vec{k}//c$.

Insert Figure 3

In Figure 4 one can see the A_4 tourmaline spectra. In this case, we used $\vec{k} \perp c$ and $\vec{k}//c$, i.e., slices cut parallel and perpendicular to the (001)-direction respectively.

Insert Figure 4

*EMBRARAD - Empresa Brasileira de Radiações S.A.

We observed the following absorption bands:

~7,000 cm^{-1} (~14,286 Å) - Sharp bands, typical harmonics of water vibrations, present in all of the observed spectra.

~8,500 cm^{-1} (~11,765 Å) - It is a wide band and is observed in the pink tourmalines A_1 and A_3 and in the green tourmaline A_4. The pink tourmaline A_2 does not exhibit this band.

~14,800 cm^{-1} (~6,768 Å) - It is a wide band well characterized in A_2 and A_3 pink tourmalines and in A_4 green tourmaline. For A_1 pink tourmaline, only a shoulder is observed.

~19,500 cm^{-1} (~5,128 Å) - This is the most important band in the visible. We can observe only in A_1, A_2 and A_3 pink tourmalines.

~23,000 cm^{-1} (~4,694 Å) - Sharp and weak bands.

~25,500 cm^{-1} (~3,922 Å) - Observed in pink tourmalines, but more visible in A_2 pink tourmaline spectra, where the UV band-edge was more displaced towards UV. For the A_1 and A_3 pink tourmalines we can see a shoulder over the UV band-edge.

In Figure 5 one can see a non-polarized optical absorption spectrum for the sample A_2, where $\vec{k} \perp c$. We observed that the 19,500 cm^{-1} band is the most affected one.

Insert Figure 5

Figure 6 shows an optical absorption spectrum for A_2 pink tourmaline where $\vec{k}//c$ using a beam polarized light. The spectrum has hardly changed with the polarization angle and the errors can be attributed to experimental conditions.

Insert Figure 6

Figure 7 shows an optical absorption spectrum for A_2 pink tourmaline where $\vec{k} \perp c$. In this case, the spectrum has varied a lot with the polarization angle for the 19,500 cm^{-1} and 25,500 cm^{-1} bands. The 19,500 cm^{-1} band moved in the UV direction and decreased with the polarization angle. We attributed that behaviour to the strong reduction of the absorption of the 19,500 cm^{-1} band showing another absorption band around 21,000 cm^{-1}.

Insert Figure 7

Figure 8 shows the absorption intensities changing with the polarization angle for the 14,800; 19,500 and 25,500 cm^{-1} bands. The pink tourmaline A_2 spectrum, where $\vec{k} \perp c$, was used. We can notice that the 19,500 and 25,500 cm^{-1} bands have a similar behaviour changing strongly with the polarization. The 14,800 cm^{-1} band is hardly affected by the polarization.

Insert Figure 8

The A_1, A_3 and A_4 tourmaline spectra present a band at 8,500 cm^{-1}, but we cannot see this band for the A_2 spectra. On the other hand the 14,800 cm^{-1} ban has an intermediate intensity in A_2, A_3 and A_4 tourmaline spectra but is weak in A_1 spectrum. From all these observations we can conclude that those two bands

are not connected to each other. Thus, the doublet hypothesis proposed by Smith[18] in those two band assignments can be eliminated. Moreover, as those two bands are observed in the A_3 and A_4 spectra, where the iron content is larger than the others, it reinforces the more accepted suggestion that those bands are iron absorption bands. On this basis we assigned the 8,500 cm^{-1} band to the Fe^{2+} -absorption in the b-site according to Faye et al.[20], Burns[21] and Burns and Simon[22]. As b-site is little distorted, the Fe^{2+} ($3d^6$) has a high spin configuration (S=2) being situated in a weak oxygen field. The energy level diagram is showed in the Figure 9. The δ and Δ_o parameters according to the scheme are:

$$\delta = 550\ cm^{-1} \qquad \Delta_o = 8{,}450\ cm^{-1} .$$

Insert Figure 9

An absorption band is observed at 13,800 cm^{-1} for A_4 green tourmaline and it is displaced to 14,800 cm^{-1} in pink tourmalines, because of the strong band-edge from the 19,500 cm^{-1} band which is the most intensive band of the pink tourmalines. According to Smith[18] the 13,800 cm^{-1} band is a doublet located at 13,400 and 13,800 cm^{-1}.

On account of the high absorption energy, we assign this band to Fe^{2+} (S=2) in c-site. This octahedral site is highly distorted. The energy level diagram is shown in Figure 10.

Insert Figure 10

The splitting shown by Smith could be assigned to the unfolding of the d_{xz} and d_{yz} levels, which is due to the

ortorhombic component of the crystal field. This assumption is reinforced by the fact that the band is present in the A_2 tourmaline spectra, which with an iron content of 250 ppm makes less probable the assumption of the Fe-Fe interaction.

The 21,000 cm^{-1} band, present in the A_2 tourmaline spectrum during the optical absorption using polarized light, can be the 21,600 cm^{-1} band observed in green tourmalines. On account of the low absorption observed, the low Fe concentration and the high absorption expected for an Fe-Fe interaction band, we adopt the same assignment as Smith does.

The sharp bands[23] at 23,000 cm^{-1} are due to the transitions $^6A_1 \rightarrow {}^4A$, ^4E belonging to the Mn^{2+}.

When we have tourmalines with high content of iron, the UV band-edge is displaced to the region of low values. In this case, we suggest that the UV band-edge is somehow related to the iron concentration, as one was observed in the yellow beryl[24].

The 19,500 cm^{-1} band is common to all the pink tourmalines. The polarization spectrum suggests that this band is related to the 25,500 cm^{-1} band. This result reinforces, the assignments of Bakhtin et al.[14] and Manning et al.[12.16,17], that they are due to Mn^{3+} ion. By analogy with epidote[25] and spodumene[26], we suggest that those bands are due to Mn^{3+} in b-site.

On the other hand the 14,800 cm^{-1} band is not polarized, reinforcing the present assignment to Fe^{2+}-ion in c-site.

IV. OPTICAL ABSORPTION SPECTRA ANALYSIS BY CRYSTAL FIELD THEORY

The Mn^{3+}-ion is stabilized in the b-site by a Jahn-Teller distortion along the O(1)H-O(3)H axis. The electric potential is:

$$V_c + V_{D4}$$

where V_c is the cubic distortion potential and V_{D4} is the tetragonal distortion potential. The matrix elements are:

$$\langle d_{x^2-y^2}|V_c|d_{x^2-y^2}\rangle = \langle d_{z^2}|V_c|d_{z^2}\rangle = 6D_q \quad ;$$

$$\langle d_{xy}|V_c|d_{xy}\rangle = \langle d_{xz}|V_c|d_{xz}\rangle = \langle d_{yz}|V_c|d_{yz}\rangle = -4D_q \quad ;$$

$$\langle d_{x^2-y^2}|V_{D4}|d_{x^2-y^2}\rangle = 2D_s - D_t \quad ;$$

$$\langle d_{z^2}|V_{D4}|d_{z^2}\rangle = -2D_s - 6D_t \quad ;$$

$$\langle d_{xy}|V_{D4}|d_{xy}\rangle = 2D_s - D_t \quad ;$$

$$\langle d_{xy}|V_{D4}|d_{xy}\rangle = \langle d_{yz}|V_{D4}|d_{yz}\rangle = -D_s + 4D_t \quad .$$

We have to consider two cases:

(a) Octahedral site compressed along the z-axis

The energy level diagram is shown in Figure 11.

Insert Figure 11

The transition energies are:

$$E(^5A_1) - E(^5B_1) = -4D_s - 5D_t$$

$$E(^5A_1) - E(^5E) = 10D_q - D_s - 10D_t = 19{,}500 \text{ cm}^{-1}$$

$$E(^5A_1) - E(^5B_2) = 10D_q - 4D_s - 5D_t = 25.500 \text{ cm}^{-1} \quad .$$

Using the value $D_q = 1{,}100 \text{ cm}^{-1}$ employed by Ito and Isotani[26], in order to explain the Mn^{3+} center in spodumene, we obtain:

$$D_t = -557 \text{ cm}^{-1}$$

$$D_s = -2{,}920 \text{ cm}^{-1} \quad .$$

The relation D_s/D_t is -5,3 and the D_s and D_t values are comparable to those obtained in spodumene. We still get:

$$E(^5A_1) - E(^5B_1) = 14{,}500 \text{ cm}^{-1} \quad .$$

This transition was not observed, probably, because it was too weak and hidden by the absorption of the Fe^{2+}-ion in the c-site.

The crystal field stabilization energy (CFSE) is given by:

$$CFSE = \frac{3}{5}(10D_q) + \frac{1}{2}\left[E(^5A_1) - E(^5B_1)\right] \quad .$$

Using the above values we get:

$$CFSE = 37.9 \text{ Kcal/mol} \quad .$$

(b) Octahedral site elongated along the z-axis

The energy level diagram is shown in Figure 12.

Insert Figure 12

The transition energies are:

$$E(^5B_1) - E(^5A_1) = 4D_s + 5D_t$$

$$E(^5B_1) - E(^5B_2) = 10D_q = 19{,}500 \text{ cm}^{-1}$$

$$E(^5B_1) - E(^5E) = 10D_q + 3D_s - 5D_t = 25{,}500 \text{ cm}^{-1} \quad .$$

Using the $D_s = 5D_t$ approximation we obtain:

$$D_q = 1{,}950 \text{ cm}^{-1}$$

$$D_s = 3{,}000 \text{ cm}^{-1}$$

$$D_t = 600 \text{ cm}^{-1}$$

$$CFSE = 54{,}9 \text{ Kcal/mol} \quad .$$

The D_q and CFSE values, compared with results obtained for other crystals[27,28], are compatible with the octahedral site compressed along the O(1)H - O(3)H axis.

Therefore, we assign the 19,500 cm^{-1} band, to the Mn^{3+} absorption in the b-site compressed along the O(1)H - O(3)H axis.

V. IRRADIATION RESULTS

The pink tourmalines A_1, A_2 and A_3 had their color accentuated by irradiation processes. The green tourmaline A_4 became pink. The variations observed in the optical absorption spectra can be seen in the Figures 13, 14, 15 and 16.

Insert Figures 13, 14, 15 and 16

We observed that the coloring process in tourmaline is reversible. The heating to 600°C for some hours changes tourmaline from pink to colorless. The lost color can be recuperated by the irradiation process.

V.a. The A_1 and A_3 pink tourmalines

The dose-curve of the 19,500 cm^{-1} band referring to the A_1 and A_3 pink tourmaline spectra, where $\vec{k}//c$ can be seen in Figure 17.

Insert Figure 17

Both present a quick initial growth, with a tendency to saturate in 2.00 MGy. Following there is another growth, forming something like a step over the first part of the growth. This new growth seems to be composed of a new saturation curve, which we name supersaturation curve and a linear growth for doses higher than those used by us in this work.

In Figure 18 we present the dose-curve of the 8,500 cm^{-1} band referring to the same tourmalines, where $\vec{k}//c$. We notice a similar behaviour to that observed to the 19,500 cm^{-1} band

with a step in 2.00 MGy.

Insert Figure 18

In the Figure 19, a dose-curve for the 25,500 cm^{-1} band is shown only for A_3 sample spectrum, where $\vec{k}//c$. For this band, a light step is observed in 2.00 MGy.

When we bleach the A_1 and A_3 pink tourmalines their spectra reveal a band at 32,000 cm^{-1} (A_1) and a shoulder at 30,000 cm^{-1} (A_3).

Insert Figure 19

V.b. A_2 pink tourmaline

This tourmaline has a low iron-concentration and a low UV band-edge. We used slices from this tourmaline, where either $\vec{k}//c$ or $\vec{k} \perp c$.

The dose-curves for the 14,800 cm^{-1} band, where $\vec{k} \perp c$ and $\vec{k}//c$, are shown in the Figure 20.

Insert Figure 20

We observe that a linear growth begins at 4.00 MGy. For $\vec{k}//c$ we note a step around 2.00 MGy, followed by the supersaturation. The dose-curves for the 25,500 cm^{-1} band, where $\vec{k}//c$ and $\vec{k} \perp c$, are shown in the Figure 21.

Insert Figure 21

We observe that from the 8.00 MGy starts a linear

growth. Here, for $\vec{k}//c$, we also notice a step in 2.00 MGy, followed by the supersaturation.

The dose-curve for the 19,500 cm^{-1} band, where $\vec{k}//c$, is shown in the Figure 22. We observe a step in 2.00 MGy, a supersaturation and a linear growth from the 8.00 MGy. In Figure 23, to $\vec{k} \perp c$, we do not observe the step, and growth is linear from the 4.00 MGy.

Insert Figures 22 and 23

In Figure 24 we show the correlation among the absorbances of the 19,500 vs 25,500 cm^{-1} bands for the A_2 pink tourmaline obtained from the dose-curves. These curves produce correlations approximately linear. The curves for $\vec{k}//c$ and $\vec{k} \perp c$ are coincident, showing the same polarization effects.

Insert Figures 24

In Figure 25, we show the correlation between the absorbances of the 19,500 cm^{-1} band measured using $\vec{k}//c$ ($A_{//}$) and $\vec{k} \perp c$ ($A_{\perp}$). We notice a deviation from the linear behaviour in D = 2.20 MGy. This deviation of the behaviour is seen in the short step in Figure 22. This supersaturation phenomenon makes difficult the analysis of the dose-curve growth.

Insert Figure 25

The dose curve, where $\vec{k} \perp c$, of the 19,500 cm^{-1} band is quite regular. Thus we made and empirical adjustment of this dose-curve. The best model to do this adjustment was Levy's model[29]:

$$y = \sum_{i=1}^{3} a_i \left(1 - e^{-\beta_i D}\right) + b \cdot D$$

where b is the angular coefficient of the linear part of the experimental curve, D is the irradiation dose to which the sample was submitted, β_i is a constant which express the i-th center growth-rate and the a_i are the contributions of each center.

The fitting curve was:

$$y = 0.954(1 - e^{-55.80D}) + 1.970(1 - e^{-13.00D}) + 1.926(1 - e^{-1.01D}) + 0.143D$$

where the dose was measured in MGy. The adjusted curve is the full line in Figure 23.

VI. DISCUSSION

We assigned to the b- and c-sites, the positions of the ions responsible for the absorptions studied by us. Let us examine the occupation possibility of the mentioned ions in those sites. The b-site is formed by the $XO_4(OH,F)_2$-octahedron. There are three sites b_1, b_2 and b_3, existing a common group (OH,F) in the O(1)H-site. The structural analysis is very complex because the X-site can be occupied by ions having charge 1+, 2+ and 3+, and the vertex of the three b-sites can be occupied by either OH^- or F^-. Let us consider, in this discussion, the b-sites from the $XO_4(OH)_2$ type. The X-ions are octahedrally

coordinated by four Oxygens in the plan perpendicular to the octahedral-axis, which has an OH^--group in each end. In the dravite the octahedron, where $X = Mg^{2+}$, is elongated along the O(1)H - O(3)H-axis[6] and the hydroxil O(1)H connects the sites b_1, b_2 and b_3. In the elbaite as X is either $A\ell^{3+}$ or Li^+ and the distortion along the O(1)H - O(3)H-axis can be quite altered.

In the elbaite, the two most probable structures for the sites b_1, b_2 and b_3 are shown in Figure 26, because of the presence of those two structures will keep the crystal neutral electrically.

Insert Figure 26

The c-sites are formed by $YO_5(OH)$-octaedra and they are occupied mainly by $A\ell^{3+}$.

The O(3)H-group is shared by a b- and a c-site. There are six c-sites in the brucite structure.

The average distance Mg-O, in dravite, in the b-site is ~ 2.06 Å and in the c-site is ~ 1.93 Å. In M(II)-oxides having structures similar to the NaCℓ, the Mg-O distance[30] is 2.25 Å. As Mn^{2+} has a d^5 configuration, it is not susceptible to Jahn-Teller distortions in six-coordination-sites. Thus the Mn^{2+} is too large to occupy the b- and c-sites. However, the structural alteration derived from the substitution of Mg by Aℓ and Li in the b-site permits us to accommodate the Mn^{2+} preferably in the b-site.

In $LaM(III)O_3$ of perovskite-structure[31,32], the Mn-O distance is ~1.97 Å, showing that the Mn^{3+} can be accommodated in the b- and c-sites, preferably in the b-site.

The Fe-O distance in $LaM(III)O_3$ is ~ 1.97 Å, so

that the Fe^{3+} can be accommodated in the b- and c-sites, preferably in the b-site. On the other hand, Fe-O distance in oxides having the same structure as NaCℓ is ~2.16 Å, therefore greater than the M-O distance in the b- and c-sites. However, Fe^{2+} is a d^6-configuration ion, susceptible to Jahn-Teller distortions in six-coordination-sites. The b- and c-sites are distorted, so that they can accommodate the Fe^{2+}.

We conclude that the b- and c-sites, can accommodate the ions Mn^{2+}, Mn^{3+}, Fe^{2+} and Fe^{3+}, with a great probability for the b-site.

Let us now analyse the results obtained from the polarization measurements and the dose-curves.

The intensities of the 19,500 and 25,500 cm^{-1} bands do not depend on the direction of $\vec{E}$ to $\vec{k}//c$. The polarization of those bands to $\vec{k} \perp c$, shows to be maximum to $\vec{E} \perp c$ and minimum to $\vec{E}//c$. As the polarization of the bands at 19,500 and 25,500 cm^{-1} shows the same features, we assigned them to the same color center. The correlations between 19,500 vs 25,500 cm^{-1} to $\vec{k}//c$ and $\vec{k} \perp c$ (Figure 24) are on the same straight line, reinforcing the assignment of these bands to only one center.

The polarization of the band at 14,800 cm^{-1} in pink tourmaline is different from that obtained for the 19,500 and 25,500 cm^{-1} bands. That is the reason why attribute its origin to another color center. In fact the 14,800 cm^{-1} band is not subject to the direction of the $\vec{E}$.

The dichroism phenomenon in the pink tourmaline, resulting from the polarization of the absorption bands was discussed by several authors. One tried to explain it by means of two models:

a) Wilkin's Model[4]:- The (111) axis of the b-site which is parallel to the c-axis, but does not coincide with the C_3 axis. This axis is situated in the brucite structure center, crossing the O(1)H-site and is parallel to the c-axis. The intensity of the absorption could be due to the expansion of the crystal field in odd terms. In this case the Hamiltonian is:

$$H_{cubic} + H_{odd\text{-}trigonal} + H_{even\text{-}tetragonal} .$$

This Hamiltonian transform itself neither according the operations from the C_3-group nor C_∞-group. Besides, it does not have the inversion symmetry in the trigonal plan. Thus, this model does not explain the polarization of the bands at 19,500 and 25,500 cm^{-1}.

b) Townsend's Model[2]:- As there is no unique distortion along $\underline{c}$, the absorption intensity dependence with the polarization should depend either on the interactions with the neighbours or on the composed spectrum symmetry.

This last one would contribute to the dichroism if the transitions within the individual b-sites were polarized along the O(1)H - O(3)H axis. The resultant spectrum would be polarized with regard to the c-axis and the absorption coefficient ratio, α, to $\vec{E}//c$ and to $\vec{E} \perp c$ would be $1<\alpha<1.73$. Nevertheless, in this model we should expect for a C_3 symmetry in the intensity of the spectrum polarized with $\vec{E}$ on the plan perpendicular to c. Besides, we should expect that the maximum values on the plan parallel to c should occur at 63° from the c-axis. Those behaviours differ from the results reported in this paper.

We observe that the band at 19,500 cm^{-1}, for the sample A_2, to $\vec{k}//c$ and $\vec{k} \perp c$ has $A_{\parallel} \sim 0.78$ and to $\vec{k} \perp c$ and $\vec{E} \perp c$, $A_{\perp} \sim 0.45$. In both cases we maintained $\vec{E} \perp c$. The difference is due to the contribution of the magnetic dipole transitions. Actually to $A_{\parallel}$ both $\vec{H}$ and $\vec{E}$ fields are perpendicular to $\underline{c}$ giving maximum contributions. To $A_{\perp}$, $\vec{E}$ is perpendicular to $\underline{c}$ giving maximum contribution, but H is parallel to c giving minimum contribution.

The heating of the pink tourmaline to 600°C for some hours produces the complete emptying of the bands responsible for the color (19,500 cm^{-1} and the UV band-edge) making it become almost colorless. By irradiation with γ-rays from C_o-60, the color is recomposed by the increasing of the absorption bands. These bands increase quickly up to 1.00 MGy when they start to be saturated.

In Figure 25, we notice two phases in the growth relation $A_{\parallel}$ vs $A_{\perp}$ of the 19,500 cm^{-1} band in the sample A_2. In the first phase up to 2.00 MGy, $A_{\parallel}$ and $A_{\perp}$ increase at the same rate keeping the relation $A_{\parallel}/A_{\perp}$ constant and is of about 1.4. Later on in the second phase $A_{\parallel}$ increases at a rate higher than $A_{\perp}$ giving a relation $A_{\perp}/A_{\parallel} > 1.4$. These observations suggest the existence of at least two color centers I and II. The center I predominates in the first growth phase of the absorption band and the center II starts to appear in significant concentrations in the second phase.

The growth of the relation $A_{\parallel}/A_{\perp}$ in the second phase is mainly due to a growth ratio more accentuated of the $A_{\parallel}$. We suggest that it is due to the fact that the center II absorbs more to $A_{\parallel}$ and less to $A_{\perp}$. As the contribution to the transition

$\vec{E} \perp c$ is the same in $A_{\parallel}$ and $A_{\perp}$, we suggest that the dichroism of the magnetic dipole transition is higher in the center II.

The dose-curves of the 19,500 cm^{-1} and 25,500 cm^{-1} bands for the samples A_1 and A_3, show phases of saturation, supersaturation and linear growth. We attribute the saturation phase to the predominant population of centers I and the supersaturation to the population of centers II.

The existence of two centers I and II is expected since the brucite structure has two possible configurations indicated in Figure 26.

ACKNOWLEDGMENTS

The authors are grateful to Mr. Beppe, J.R.M. Fortunato and M. Blum for the samples, to Prof. O.L. Dias (UFGo) for the X-ray fluorescence measurements, to EMBRARAD S.A. for the use of their 60 γ-rays source and to Prof. Dr. Walter M. Pontuschka for the discussions which enriched this work.

This work was supported by grants of CAPES, CNPq, FAPESP and FINEP.

REFERENCES

1) R. Barton Jr., Acta Cryst. B25, 1524 (1969).
2) M.G. Townsend, J. Phys. Chem. Solids 1, 2481 (1970).
3) R. Webster, Gems, their sources, description and identification, 2nd ed., Butterworths, London, Boston (1980).
4) R.W.T. Wilkins, E.F. Farrel, and C.S. Naiman, J. Phys. Chem. Solids 30, 43 (1969).
5) N.V. Belov and E.N. Belova, Dokl. Akad. Nauk S.S.S.R. 75, 807 (1950).
6) M.J. Buerger, C.W. Burnham, and D.R. Peacok, Acta Cryst. 15, 583 (1962).
7) G. Donnay and R. Barton, Tschermaks Min. Petr. Mitt. 18, 273 (1972).
8) G. Donnay and M.J. Buerger, Acta Cryst. 3, 379 (1950).
9) G.E. Hambuerger and M.J. Buerger, Amer. Mineral. 33, 532 (1948).
10) T. Ito and R. Sadanaga, Acta Cryst. 4, 385 (1951).
11) J.E.S. Bradley and O. Bradley, Mineral. Mag. 30, 26 (1953).
12) P.G. Manning, Can. Mineral. 9, 678 (1969).
13) M.S. Slivko, Miner. Sbornik. Lvov. Geol. Obsh. 13, 139, translated in Internat. Geol. Rev., 195 (1961).
14) A.I. Bakhtin, O.Ye. Minko, and V.M. Vikonurov, Izv. Akad. Nauk. S.S.S.R., Ser. Geol. 6, 73 (1975).
15) L.V. Bershov, V.O. Martirosyan, A.S. Marfunin, A.N. Platonov, and A.N. Tarashchan, Soviet. Phys. Cryst. 13, 629 (1969).
16) P.G. Manning, Can. Mineral. 9, 348 (1968).
17) P.G. Manning, Can. Mineral. 11, 971 (1973).
18) G. Smith, Phys. Chem. Minerals 3, 343 (1978).
19) K. Nassau, Amer. Mineral. 60, 710 (1975).

20) G.H. Faye, P.G. Manning, and E.H. Nickel, Amer. Mineral. 53, 1174 (1968).

21) R.G. Burns, Can. J. Spectrosc. 17, 51 (1972).

22) R.G. Burns and H.F. Simon, Geol. Soc. Amer. Ann. Mtg,Abstract 5, 563 (1973).

23) D.S. MacClure, Sol. State Phys. 9, 399 (1959).

24) S. Isotani, O.L. Dias, and A.R.P.L. Albuquerque, "Optical Absorption in Irradiated Natural Beryl", preprint IFUSP/P-436.

25) R.G. Burns and R.G.J. Strens, Min. Mag. 35, 547 (1967).

26) A.S. Ito and S. Isotani, "Optical Absorption and Electron Spin Resonance in Natural, Irradiated and Heated Spodumene", preprint IFUSP/P-429.

27) J.D. Dunitz and L.E. Orgel, J. Phys. Chem. Solids 3, 318 (1957).

28) D.S. MacClure, J. Phys. Chem. Solids 3, 311 (1957).

29) P.W. Levy, P.L. Mattern, K. Lengweiler, and A. Bishay, J. Am. Ceramic Soc. 57, 176 (1974).

30) N.S. Hush, Disc. Faraday Soc. 26, 145 (1958).

31) N.S. Hush and M.H.L. Pryce, J. Chem. Phys. 26, 143 (1957).

32) N.S. Hush and M.H.L. Pryce, J. Chem. Phys. 28, 424 (1958).

TABLE 1 - Summary from the assignments to the optical absorption of the rubellite.

Optical Absorption Band	Assignments
$\vec{E}//c$, $\vec{E}\perp c$ 7,000 cm^{-1} (-14,286 Å)	molecular vibrations of the OH^- ion and/or H_2O; Wilkins[4].
$\vec{E}\perp c$ - 12,200 cm^{-1} (-8,197 Å) $\vec{E}\perp c$, $\vec{E}//c$ 13,900 cm^{-1} (-7,194 Å)	unfolded transition $^6A_1 \rightarrow {}^4A_1$ in Mn^{2+} and Fe^{3+}; Wilkins[4].
$\vec{E}\perp c$ - 17,200 cm^{-1} (-5,814 Å)	hardly defined band in the spectrum shoulder transition $^6A_1 \rightarrow {}^4T_2(G)$ in Mn^{2+} and Fe^{3+} in b-sites; Wilkins[4].
$\vec{E}\perp c$, $\vec{E}//c$ 19,200 cm^{-1} (-5,208 Å)	absorption due to Mn cation; Slivko[13].
	transition $^6A_1 \rightarrow {}^4T_2(G)$ in Mn^{2+} and Fe^{3+} in b-sites; Wilkins[4].
	transition $^5E \rightarrow {}^5T_2(D)$* in Mn^{3+} bounded octahedrally; Manning[12,16,17].
	color centers of the electron-hole type; Bershov[15].
	Mn^{3+}; Bakhtin[14]
	defects in the lattice; Smith[18].

*This transition is inverted.

cont.

cont.

Optical Absorption Band	Assignments
21,900 cm^{-1} (~4,566 Å) and 22,200 cm^{-1} (~4,505 Å)	($\vec{E}$//c and $\vec{E}\perp$c), transitions $^6A_1 \rightarrow {}^4A_1, {}^4E$ independent of the field in the Mn^{2+}; Wilkins[4].
	($\vec{E}\perp$c), electronic transitions $^6A_1 \rightarrow {}^4A_1, {}^4E(G)$ in the Fe^{3+} bounded octahedrally. ($\vec{E}$//c), shoulder observed in 21,000 cm^{-1}, Jahn-Teller effect originated from the $t_{2g}^{(3)} e_g^{(1)}$ configuration of the Mn^{3+} ($3d^4$); Manning[12].
$\vec{E}\perp$c, $\vec{E}$//c 24,500 cm^{-1} (~4,082 Å)	spin forbidden transitions for several triplet levels in the Mn^{3+}; Manning[12].

TABLE 2 - Concentrations of transition metal impurities in the pink and green tourmalines for X-ray fluorescence.

Sample	Color	Fe-content (p.p.m.)	Mn-content (p.p.m.)	Ratio (Mn/Fe)
A_1	pink	386 ± 30	11,050 ± 30	28.6
A_2	pink	250 ± 20	8,690 ± 30	34.8
A_3	pink	700 ± 20	11,750 ± 30	16.8
A_4	green	7,450 ± 500	9,000 ± 30	1.2

FIGURE CAPTIONS

Figure 1 - The upper layer of the structure made up from consisting octahedra. The central three larger octahedra contain X-atoms at the centre. The six smaller peripherical octahedra contain Aℓ. The small circles are B atoms bounded along the broken lines to the corners of octahedra. The lower right octahedron in the first figure is pierced by a 3_1 screw axis. In the second figure, we see the manner in which the various octahedral layers of the structure are joined to each other.

Figure 2 - Cut of the tourmaline samples for the optical absorption measurements.

Figure 3 - Optical absorption spectra of three pink tourmalines (samples cut perpendicular to the c-axis).

Figure 4 - Optical absorption spectra of the green tourmaline (sample A_4 cut parallel and perpendicular to the crystallographic axis).

Figure 5 - Optical absorption spectrum of the pink tourmaline A_2 (sample cut parallel to the c-axis).

Figure 6 - Polarization measurements, sample A_2 cut perpendicular to the c-axis.

Figure 7 - Polarization measurements, sample A_2 cut parallel to the c-axis.

Figure 8 - Behaviour of the absorption bands with the variation of the electric field direction throughout polaroids (sample A_2 cut parallel to c).

Figure 9 - Energy level diagram of the Fe^{2+} in the b-site.

Figure 10 - Energy level diagram of the Fe^{2+} in the c-site.

Figure 11 - Energy level diagram of the Mn^{3+} in a compressed octahedron along the z-axis.

Figure 12 - Energy level diagram of the Mn^{3+} in an elongated octahedron along the z-axis.

Figure 13 - Growth of the absorption bands with the irradiation dose for the sample A_1 cut perpendicular to the c-axis (plan 001).

Figure 14 - Growth of the absorption bands with the irradiation dose for the sample A_2 cut perpendicular to the c-axis (plan 001).

Figure 15 - Growth of the absorption bands with the irradiation dose for the sample A_2 cut parallel to the c-axis.

Figure 16 - Growth of the absorption bands with the irradiation dose for the sample A_3 cut perpendicular to the c-axis (plan 001).

Figure 17 - Growth of the 19,500 cm^{-1} band with the irradiation dose. Samples A_1 and A_3 cut perpendicular to the c-axis.

Figure 18 - Growth of the 8,500 cm^{-1} band with the irradiation dose. Samples A_1 and A_3 cut perpendicular to the c-axis.

Figure 19 - Growth of the 25,500 cm^{-1} band with the irradiation dose. Sample A_3 perpendicular to the c-axis.

Figure 20 - Growth of the 14,800 cm^{-1} band with the irradiation dose. Sample A_2 cut parallel and perpendicular to the c-axis.

Figure 21 - Growth of the 25,500 cm^{-1} band with the irradiation dose. Sample A_2 cut parallel and perpendicular to the c-axis.

Figure 22 - Growth of the 19,500 cm^{-1} band with the irradiation dose. Sample A_2 cut perpendicular to the c-axis.

Figure 23 - Growth of the 19,500 cm^{-1} band with the irradiation dose adjusted according to Levy's model for the sample A_2 cut parallel to the c-axis.

Figure 24 - Correlation between the growth of the 19,500 and 25,500 cm^{-1} bands in function of the irradiation dose. Sample A_2.

Figure 25 - Correlation between the growth of $A_{\parallel}$ and $A_{\perp}$ in function of the irradiation dose, for the 19,500 cm^{-1} band. Sample A_2.

Figure 26 - Sketch of the two possible structures for the b-sites in elbaite.

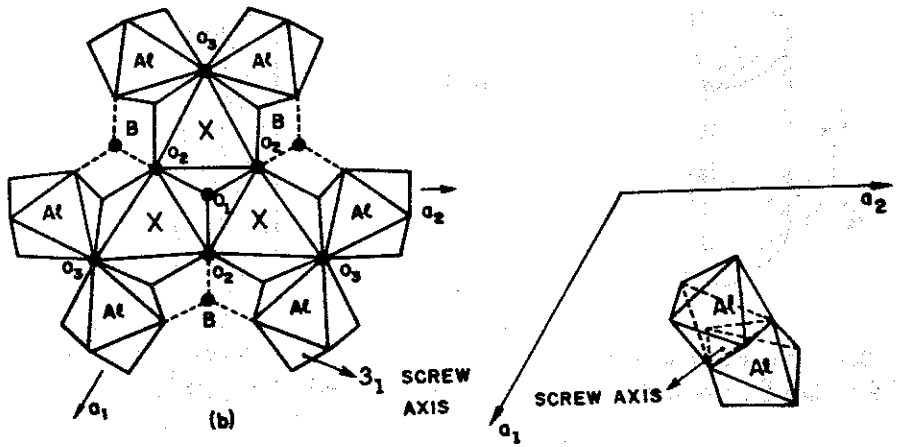

Figure 1 - The upper layer of the structure made up from consisting octahedra. The central three larger octahedra contain X-atoms at the centre. The six smaller peripherical octahedra contain Aℓ. The small circles are B atoms bounded along the broken lines to the corners of octahedra. The lower right octahedron in the first figure is pierced by a 3_1 screw axis. In the second figure, we see the manner in which the various octahedral layers of the structure are joined to each other.

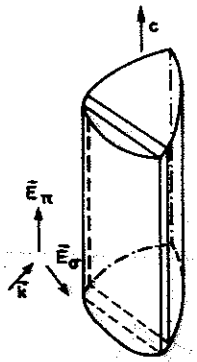

Cut in the plan // c, with $\vec{k} \perp c$ and $\vec{E} \perp c$ or $\vec{E} // c$.

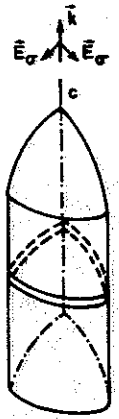

Cut in the plan 001 (⊥c), with $\vec{k} // c$ and $\vec{E} \perp c$.

Figure 2 - Cut of the tourmaline samples for the optical absorption measurements.

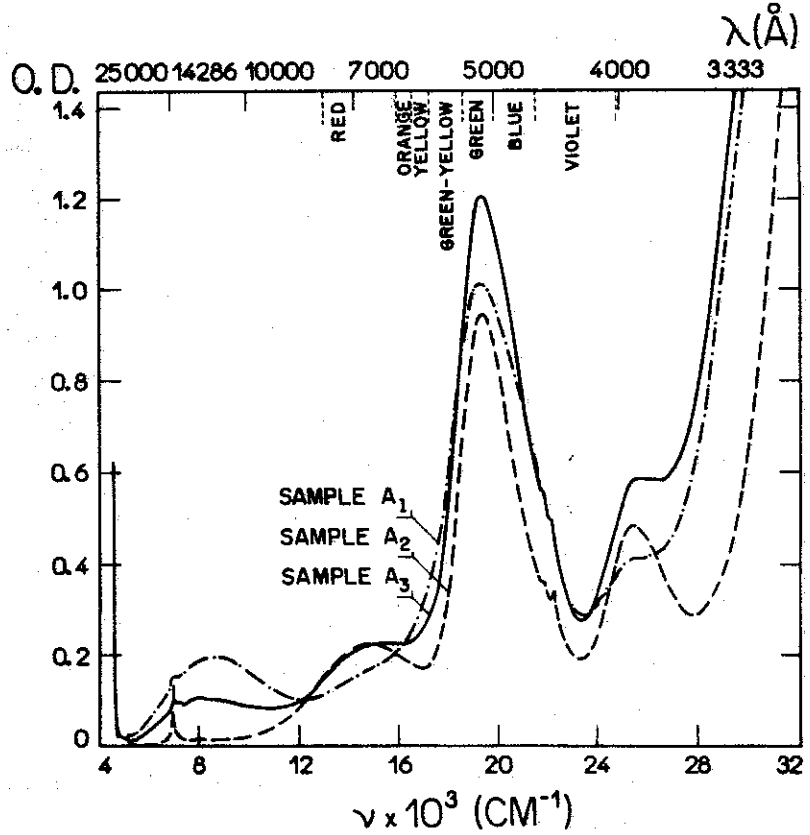

Figure 3 - Optical absorption spectra of three pink tourmalines (samples cut perpendicular to the c-axis).

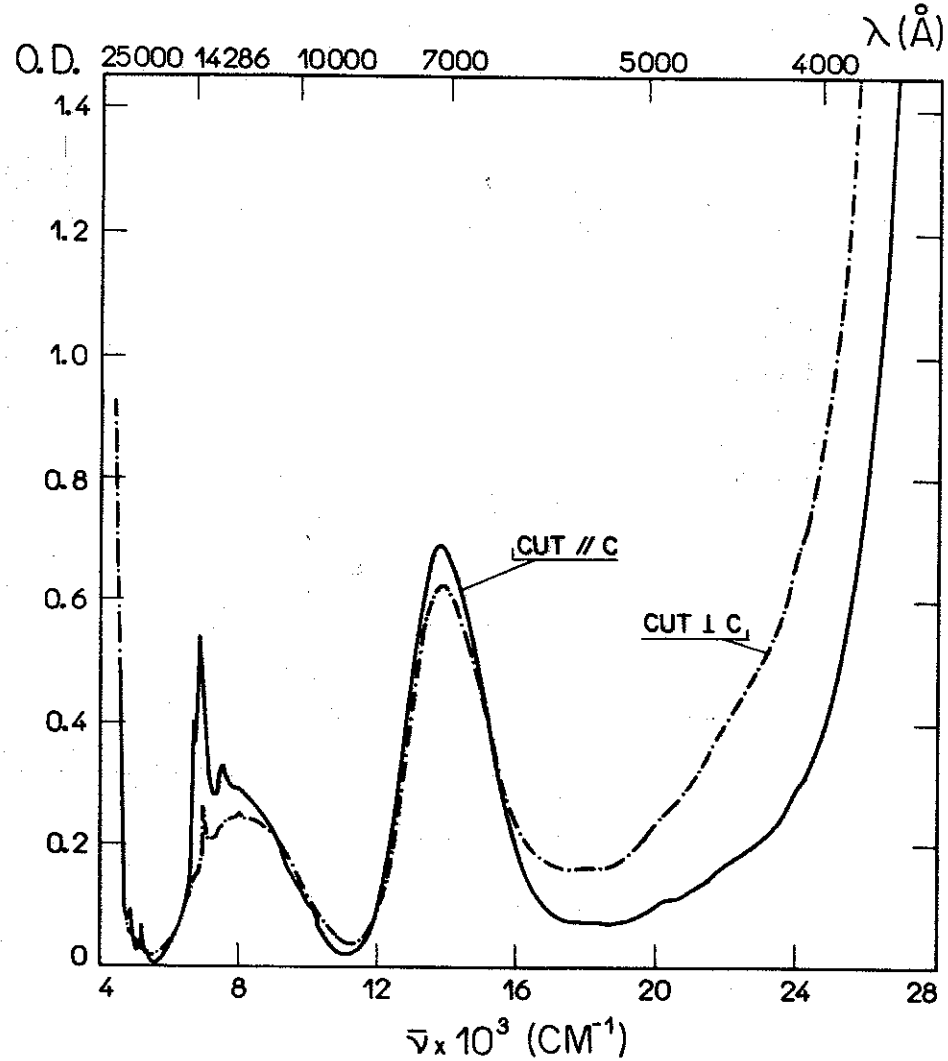

Figure 4 - Optical absorption spectra of the green tourmaline (sample A_4 cut parallel and perpendicular to the crystallographic axis).

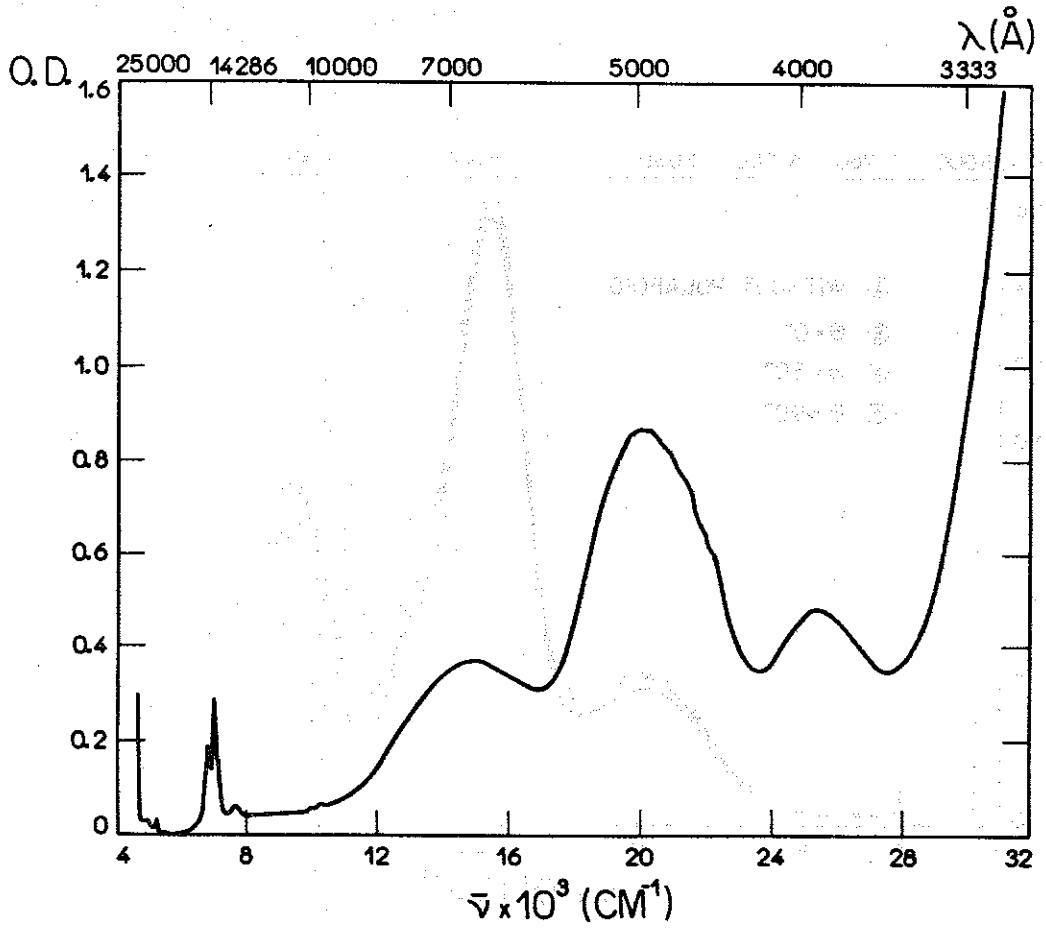

Figure 5 - Optical absorption spectrum of the pink tourmaline A_2 (sample cut parallel to the c-axis).

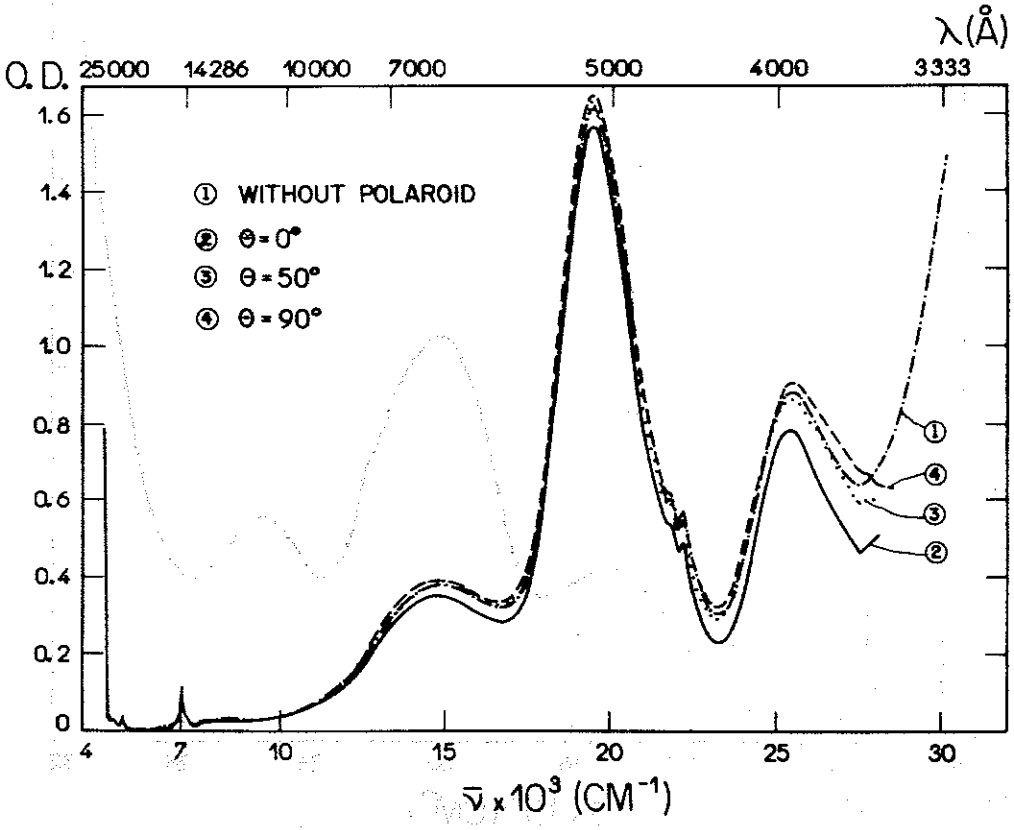

Figure 6 - Polarization measurements, sample A_2 cut perpendicular to the c-axis.

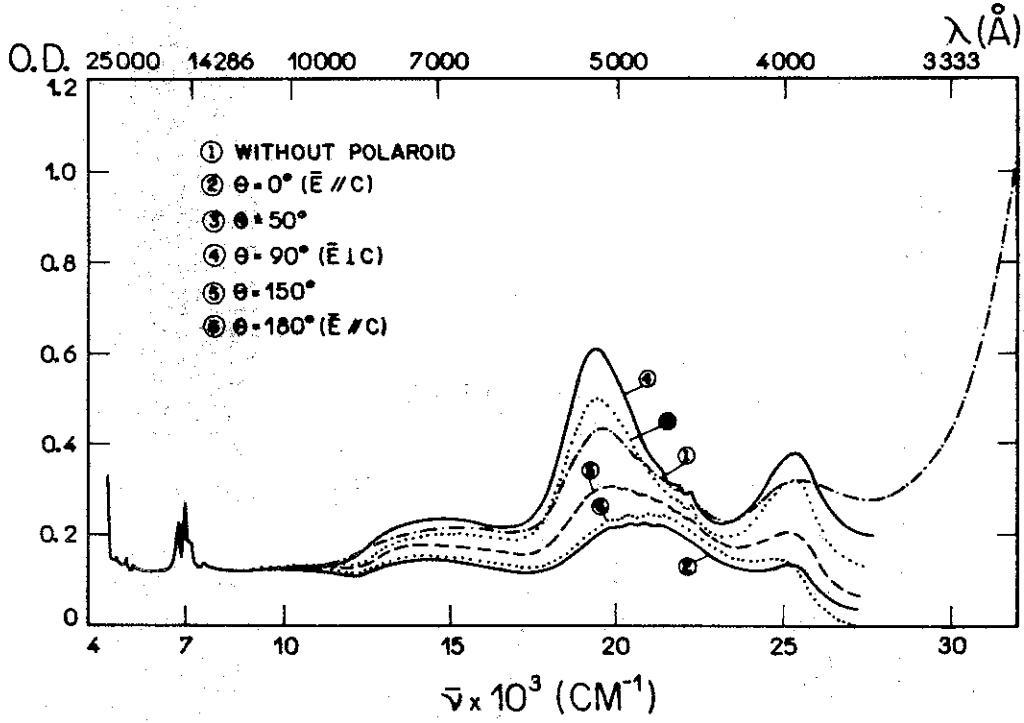

Figure 7 - Polarization measurements, sample A_2 cut parallel to the c-axis.

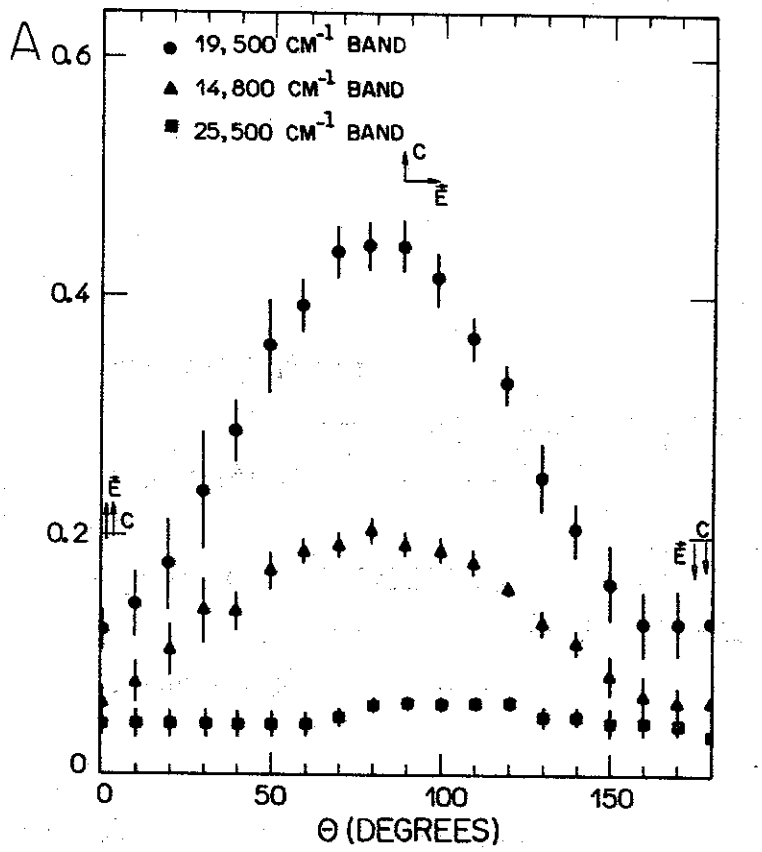

Figure 8 - Behaviour of the absorption bands with the variation of the electric field direction throughout polaroids (sample A_2 cut parallel to c).

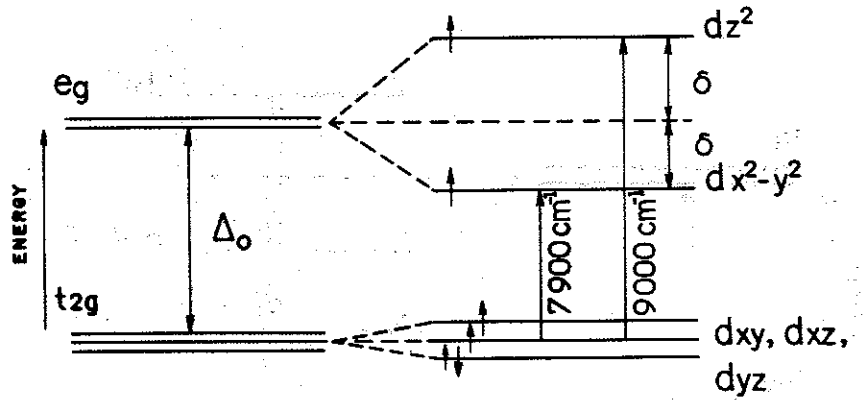

Figure 9 - Energy level diagram of the Fe^{2+} in the b-site.

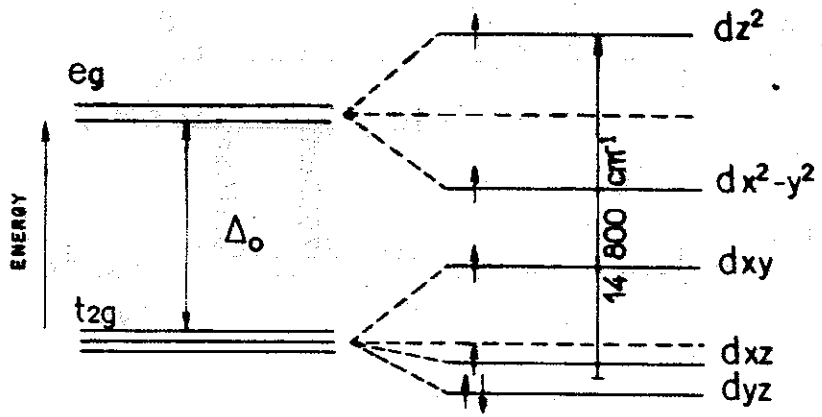

Figure 10 - Energy level diagram of the Fe^{2+} in the c-site.

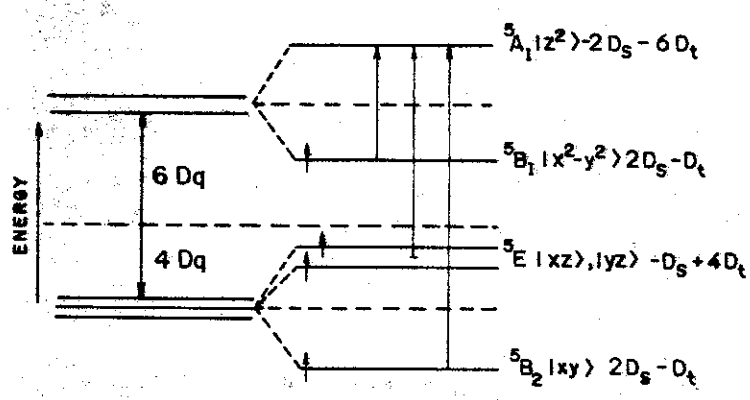

Figure 11 - Energy level diagram of the Mn^{3+} in a compressed octahedron along the z-axis.

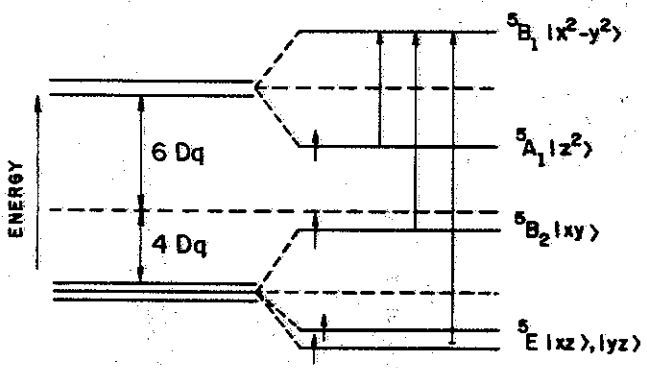

Figure 12 - Energy level diagram of the Mn^{3+} in an elongated octahedron along the z-axis.

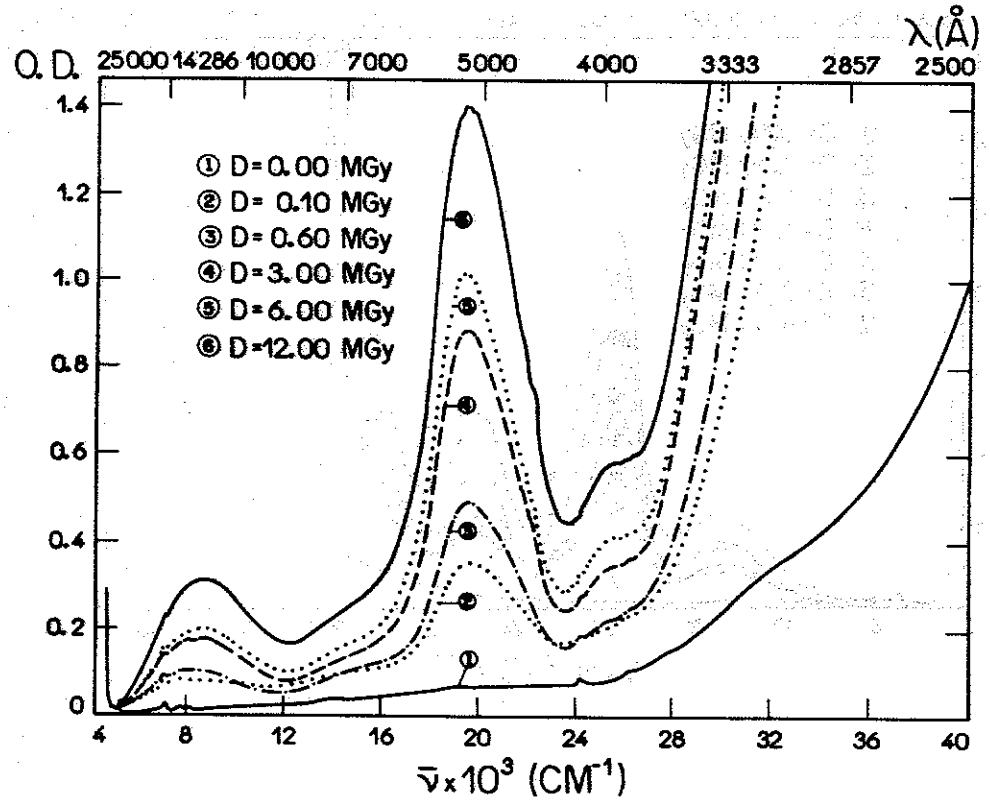

Figure 13 - Growth of the absorption bands with the irradiation dose for the sample A_1 cut perpendicular to the c-axis (plan 001).

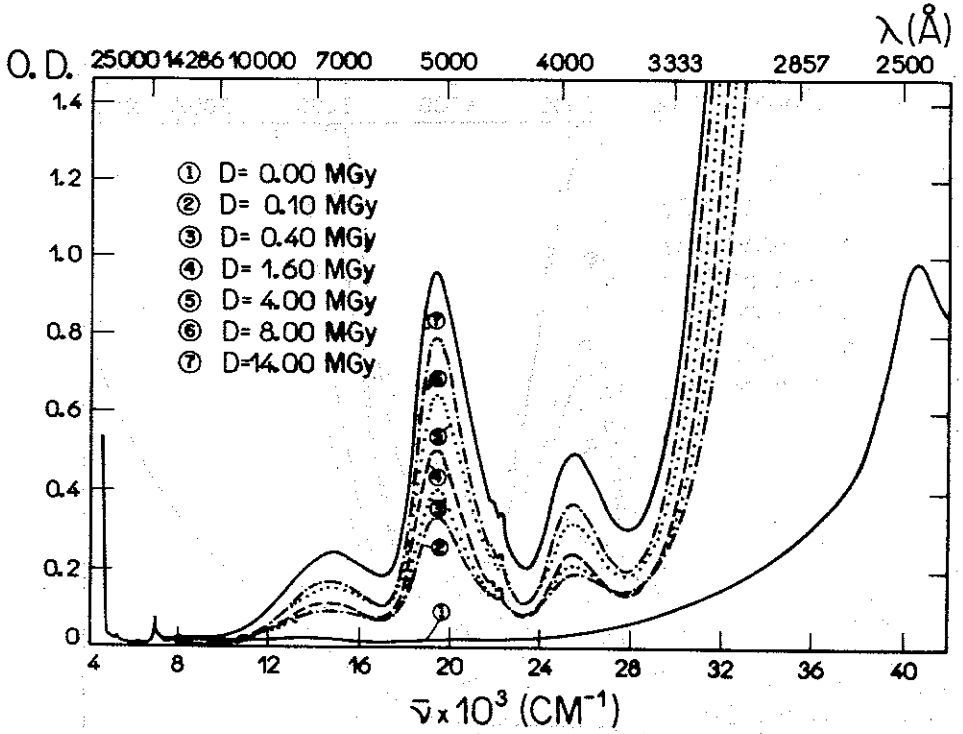

Figure 14 - Growth of the absorption bands with the irradiation dose for the sample A_2 cut perpendicular to the c-axis (plan 001).

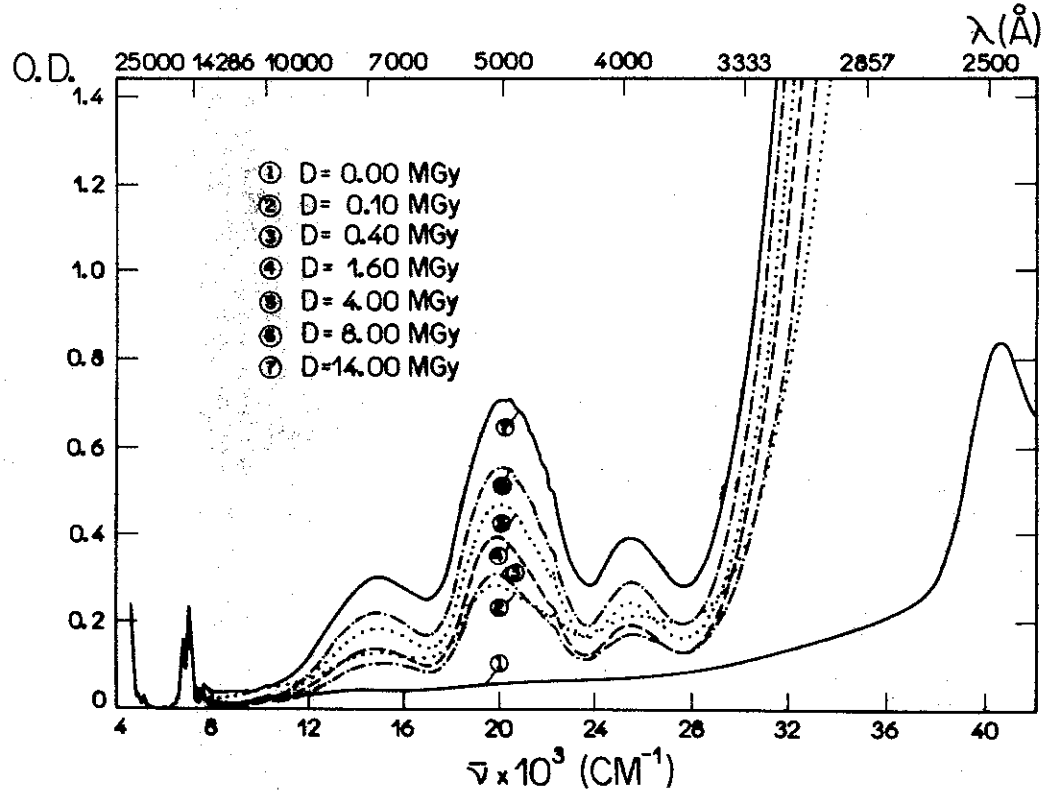

Figure 15 - Growth of the absorption bands with the irradiation dose for the sample A_2 cut parallel to the c-axis.

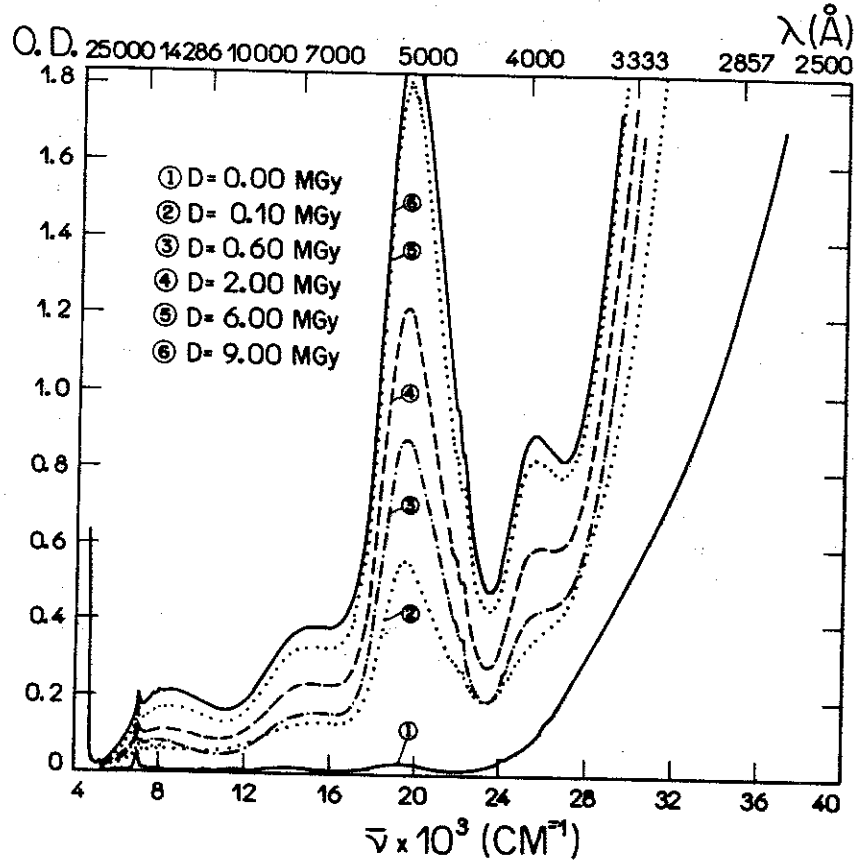

Figure 16 - Growth of the absorption bands with the irradiation dose for the sample A_3 cut perpendicular to the c-axis (plan 001).

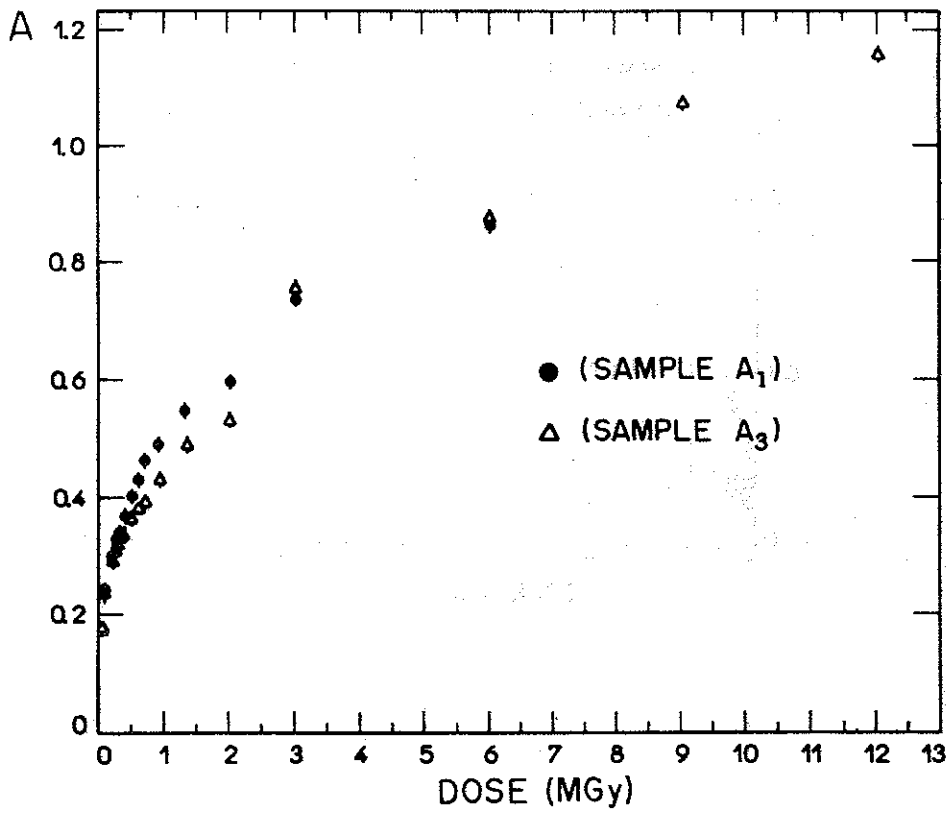

Figure 17 - Growth of the 19,500 cm^{-1} band with the irradiation dose. Samples A_1 and A_3 cut perpendicular to the c-axis.

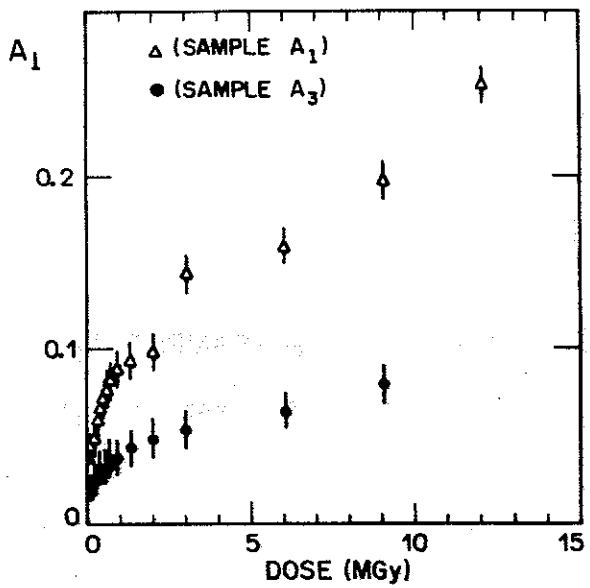

Figure 18 - Growth of the 8,500 cm^{-1} band with the irradiation dose. Samples A_1 and A_3 cut perpendicular to the c-axis.

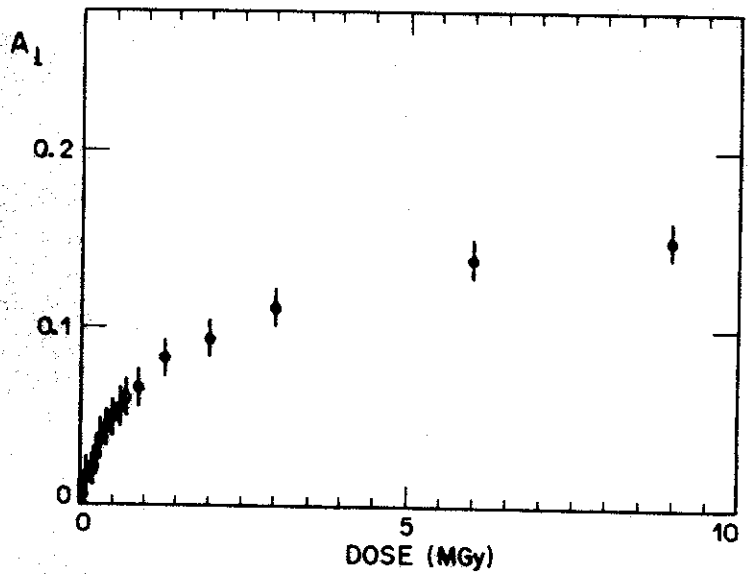

Figure 19 - Growth of the 25,500 cm^{-1} band with the irradiation dose. Sample A_3 perpendicular to the c-axis.

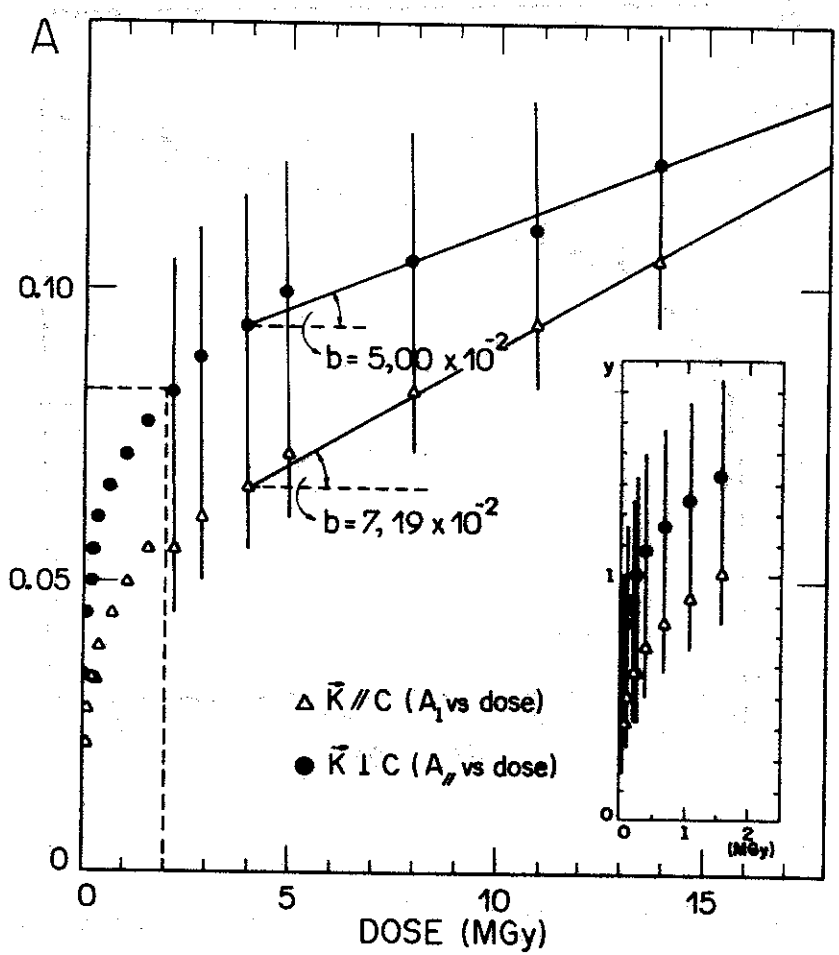

Figure 20 - Growth of the 14,800 cm^{-1} band with the irradiation dose. Sample A_2 cut parallel and perpendicular to the c-axis.

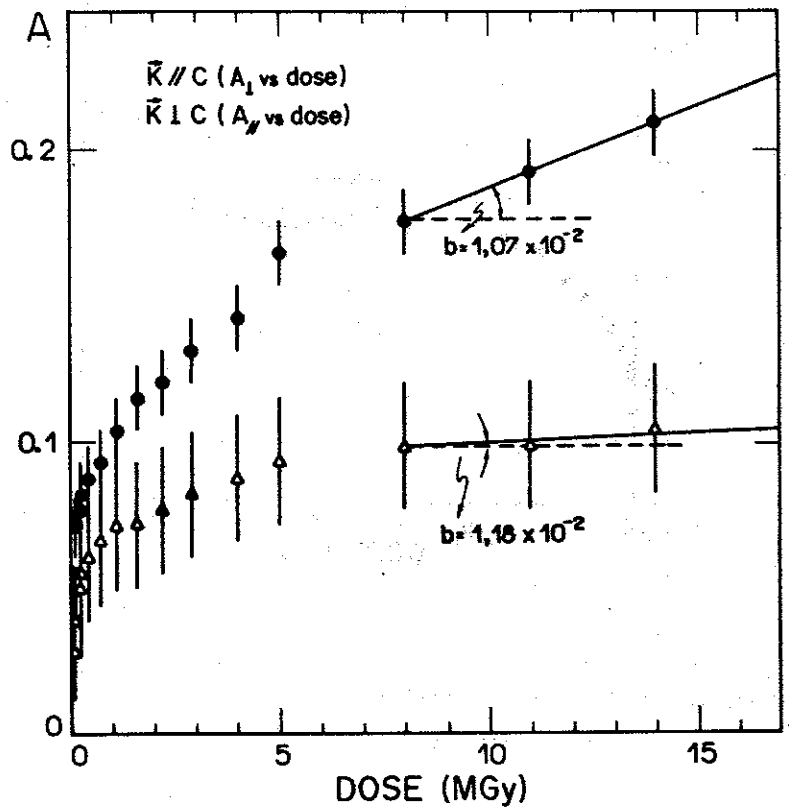

Figure 21 - Growth of the 25,500 cm^{-1} band with the irradiation dose. Sample A_2 cut parallel and perpendicular to the c-axis.

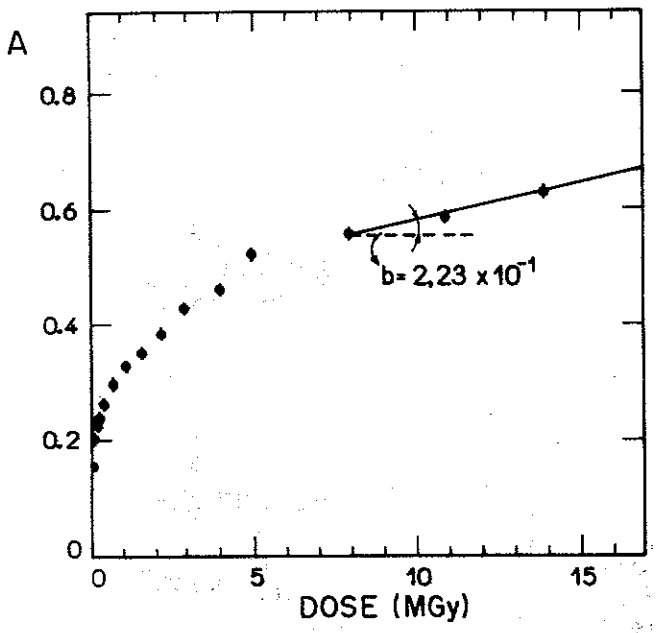

Figure 22 - Growth of the 19,500 cm^{-1} band with the irradiation dose. Sample A_2 cut perpendicular to the c-axis.

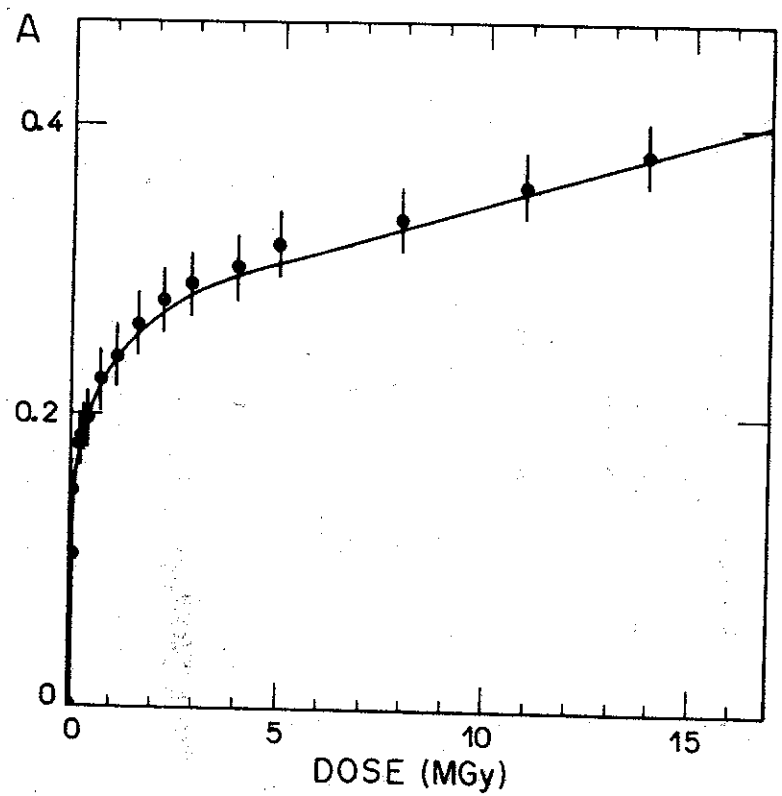

Figure 23 - Growth of the 19,500 cm^{-1} band with the irradiation dose adjusted according to Levy's model for the sample A_2 cut parallel to the c-axis.

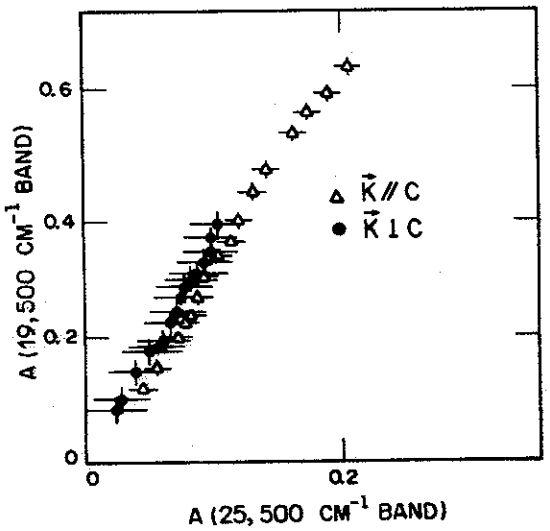

Figure 24 - Correlation between the growth of the 19,500 and 25,500 cm^{-1} bands in function of the irradiation dose. Sample A_2.

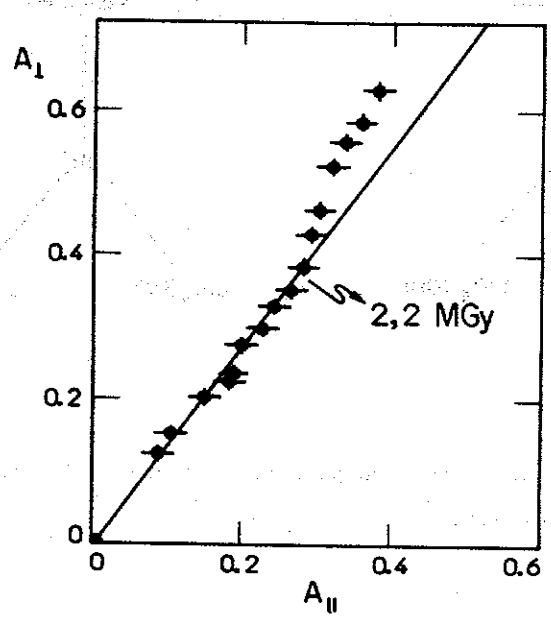

Figure 25 - Correlation between the growth of A_{II} and $A_\perp$ in function of the irradiation dose, for the 19,500 cm^{-1} band. Sample A_2.

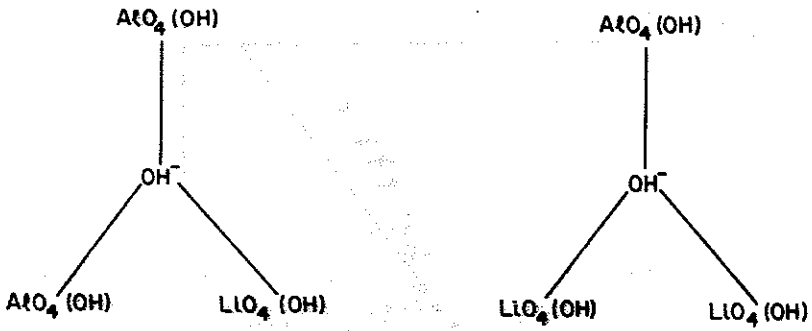

Figure 26 - Sketch of the two possible structures for the b-sites in elbaite.